Inorg. Chem. **2008**, *47*, 297–305

Ternary Rare-Earth Manganese Bismuthides: Structures and Physical Properties of RE_3MnBi_5 (RE = La–Nd) and $Sm_2Mn_3Bi_6$

Oksana Ya. Zelinska[†,‡] and Arthur Mar*[,†]

Department of Chemistry, University of Alberta, Edmonton, Alberta, Canada T6G 2G2, and Department of Inorganic Chemistry, Ivan Franko National University of Lviv, 79005 Lviv, Ukraine

Received July 18, 2007

Investigations in the ternary RE–Mn–Bi systems where RE is an early rare earth element have revealed the existence of the polybismuthides RE_3MnBi_5 (RE = La–Nd), previously known only for the Ce member, and the new compound $Sm_2Mn_3Bi_6$. Their structures were determined from single-crystal X-ray diffraction data. The RE_3MnBi_5 compounds adopt the hexagonal inverse Hf_5Cu_3Sn-type structure (Pearson symbol *hP*18, space group $P6_3/mcm$, a = 9.7139(11)–9.5438(16) Å, c = 6.4883(7)–6.4089(11) Å for RE = La–Nd), containing chains of face-sharing Mn-centered octahedra. $Sm_2Mn_3Bi_6$ adopts a new monoclinic structure type (Pearson symbol *mP*22, space group $P2_1/m$, a = 10.3917(8) Å, b = 4.4557(3) Å, c = 13.2793(10) Å, β = 108.0100(10)°) in which the Mn centers are coordinated by Bi atoms in diverse geometries (distorted octahedral, trigonal bipyramidal, and distorted tetrahedral (seesaw)) and participate in extensive metal–metal bonding in the form of chains of Mn_3 clusters. Homoatomic bonding interactions involving nominally anionic Bi atoms are manifested as one-dimensional Bi chains in RE_3MnBi_5 and as four-atom-wide Bi ribbons in $Sm_2Mn_3Bi_6$. Electrical resistivity measurements on single crystals revealed metallic behavior with prominent transitions near 40 K for RE_3MnBi_5 and 50 K for $Sm_2Mn_3Bi_6$. Magnetic susceptibility measurements showed that Pr_3MnBi_5 undergoes magnetic ordering near 25 K.

Introduction

Ternary rare-earth antimonides that are Sb-rich often possess structures that feature extensive polyanionic networks of Sb atoms in the form of chains, ribbons, or nets.[1] Extension to the polybismuthides is more challenging because Bi, with its lower electronegativity, is less disposed to adopt formally negative oxidation states.[2] Indeed, compared to the antimonides,[3] understanding of ternary rare-earth bismuthides remains very much underdeveloped.[4] For example, in the RE−Mn−Sb systems, several phases are known: RE_6MnSb_2 (RE = Ho, Er, Lu),[5,6] $RE_{14}MnSb_{11}$ (RE = Eu, Yb),[7,8] $Eu_{10}Mn_6Sb_{13}$,[9,10] $REMn_2Sb_2$ (RE = Eu, Yb),[11,12] $REMn_{1-x}Sb_2$ (RE = La−Nd, Sm),[13−15] and RE_6MnSb_{15} (RE = La, Ce).[16,17] In contrast, in the RE−Mn−Bi systems, only RE_6MnBi_2 (RE

* To whom correspondence should be addressed. E-mail: arthur.mar@ualberta.ca.
† University of Alberta.
‡ Ivan Franko National University of Lviv.

(1) Mills, A. M.; Lam, R.; Ferguson, M. J.; Deakin, L.; Mar, A. *Coord. Chem. Rev.* **2002**, *233*−*234*, 207−222.
(2) Morgan, M. G.; Wang, M.; Chan, W. Y.; Mar, A. *Inorg. Chem.* **2003**, *42*, 1549−1555.
(3) Sologub, O. L.; Salamakha, P. S. In *Handbook on the Physics and Chemistry of Rare Earths*; Gschneidner, K. A., Jr., Bünzli, J.-C. G., Pecharsky, V. K., Eds.; Elsevier: Amsterdam, 2003; Vol. 33, pp 1−223.
(4) Mar, A. In *Handbook on the Physics and Chemistry of Rare Earths*; Gschneidner, K. A., Jr., Bünzli, J.-C. G., Pecharsky, V. K., Eds.; Elsevier: Amsterdam, 2006; Vol. 36, pp 1−82.
(5) Morozkin, A. V. *J. Alloys Compd.* **2003**, *360*, L1−L2.
(6) Morozkin, A. V.; Nirmala, R.; Malik, S. K. *J. Alloys Compd.* **2005**, *394*, 75−79.
(7) Chan, J. Y.; Wang, M. E.; Rehr, A.; Kauzlarich, S. M.; Webb, D. J. *Chem. Mater.* **1997**, *9*, 2131−2138.
(8) Chan, J. Y.; Olmstead, M. M.; Kauzlarich, S. M.; Webb, D. J. *Chem. Mater.* **1998**, *10*, 3583−3588.
(9) Holm, A. P.; Park, S.-M.; Condron, C. L.; Olmstead, M. M.; Kim, H.; Klavins, P.; Grandjean, F.; Hermann, R. P.; Long, G. J.; Kanatzidis, M. G.; Kauzlarich, S. M.; Kim, S.-J. *Inorg. Chem.* **2003**, *42*, 4660−4667.
(10) Brown, D. E.; Johnson, C. E.; Grandjean, F.; Hermann, R. P.; Kauzlarich, S. M.; Holm, A. P.; Long, G. J. *Inorg. Chem.* **2004**, *43*, 1229−1234.
(11) Rühl, R.; Jeitschko, W. *Mater. Res. Bull.* **1979**, *14*, 513−517.
(12) Morozkin, A. V.; Isnard, O.; Henry, P.; Granovsky, S.; Nirmala, R.; Manfrinetti, P. *J. Alloys Compd.* **2006**, *420*, 34−36.
(13) Cordier, G.; Schäfer, H.; Woll, P. *Z. Naturforsch. B: Anorg. Chem. Org. Chem.* **1985**, *40*, 1097−1099.
(14) Sologub, O.; Hiebl, K.; Rogl, P.; Bodak, O. *J. Alloys Compd.* **1995**, *227*, 40−43.

10.1021/ic701428p CCC: $40.75
Published on Web 12/06/2007

Table 1. Crystallographic Data for RE_3MnBi_5 (RE = La−Nd) and $Sm_2Mn_3Bi_6$

formula	La_3MnBi_5	Ce_3MnBi_5	Pr_3MnBi_5	Nd_3MnBi_5	$Sm_2Mn_3Bi_6$
formula mass (amu)	1516.57	1520.20	1522.57	1532.56	1719.40
space group	*P6*$_3$/*mcm* (No. 193)	*P6*$_3$/*mcm* (No. 193)	*P6*$_3$/*mcm* (No. 193)	*P6*$_3$/*mcm* (No. 193)	*P*2$_1$/*m* (No. 11)
T (°C)	−80	−80	−80	−80	22
a (Å)	9.7139(11)	9.6229(8)	9.5849(11)	9.5438(16)	10.3917(8)
b (Å)	9.7139	9.6229	9.5849	9.5438	4.4557(3)
c (Å)	6.4883(7)	6.4420(6)	6.4311(8)	6.4089(11)	13.2793(10)
β (deg)	90.00	90.00	90.00	90.00	108.0100(10)
V (Å^3)	530.21(10)	516.61(8)	511.67(10)	505.54(15)	584.74(7)
Z	2	2	2	2	2
ρ_{calcd} (g cm^{-3})	9.499	9.773	9.882	10.068	9.766
radiation	Mo Kα, λ = 0.710 73 Å	Mo Kα, λ = 0.710 73 Å	Mo Kα, λ = 0.710 73 Å	Mo Kα, λ = 0.710 73 Å	Mo Kα, λ = 0.710 73 Å
μ (mm^{-1})	95.52	98.84	100.74	102.91	102.84
2θ range (deg)	4.84−66.20	4.88−52.68	4.90−66.26	4.92−66.00	3.22−66.28
no. of data collected	5813 (R_{int} = 0.074)	3764 (R_{int} = 0.045)	6447 (R_{int} = 0.077)	5508 (R_{int} = 0.097)	8154 (R_{int} = 0.069)
no. of unique data	393 (344 with $F^2 > 2\sigma(F^2)$)	214 (209 with $F^2 > 2\sigma(F^2)$)	380 (360 with $F^2 > 2\sigma(F^2)$)	375 (319 with $F^2 > 2\sigma(F^2)$)	2416 (1959 with $F^2 > 2\sigma(F^2)$)
no. of variables	14	14	14	14	68
$R(F)$ ($F^2 > 2\sigma(F^2)$)[a]	0.022	0.014	0.025	0.030	0.037
$R_w(F^2)$[a]	0.049	0.033	0.057	0.061	0.081
goodness of fit	1.183	1.302	1.128	1.166	1.051

[a] $R(F) = \sum||F_o| - |F_c||/\sum|F_o|$; $R_w(F_o^2) = [\sum[w(F_o^2 - F_c^2)^2]/\sum wF_o^4]^{1/2}$, $w^{-1} = [\sigma^2(F_o^2) + (Ap)^2 + Bp]$, where $p = [\max(F_o^2,0) + 2F_c^2]/3$.

= Dy−Tm, Lu, Y),[5,18,19] $RE_{14}MnBi_{11}$ (RE = Eu, Yb),[7,8] and Ce_3MnBi_5[20] are known. The last compound, Ce_3MnBi_5, adopts a structure (inverse Hf_5Cu_3Sn-type) whose one-dimensional character imparts anisotropic properties that have been studied in other related phases.[21−26] Moreover, given the large number of f and d electrons available in these rare-earth manganese bismuthides, interesting magnetic properties may be anticipated.

We present here the complete range of RE substitution in RE_3MnBi_5 (RE = La−Nd) and the new polybismuthide $Sm_2Mn_3Bi_6$, which adopts an original structure type involving extensive Bi−Bi bonding and diverse Mn coordination geometries. We also report the electrical and magnetic properties for some of these members, and probe the bonding in these compounds through band structure calculations.

Experimental Section

Synthesis. Starting materials were RE pieces (99.9%, Alfa-Aesar, Cerac, or Sigma-Aldrich), Mn powder (99.95%, Cerac), and Bi pieces (99.999%, Cerac). The elements were mixed in stoichiometric ratios and loaded into alumina crucibles placed within sealed and evacuated fused-silica tubes. For RE_3MnBi_5, the samples were heated at 850 °C for 4 days and cooled to 20 °C over 5 days. For $Sm_2Mn_3Bi_6$, the sample was heated at 850 °C for 4 days, cooled to 400 °C over 4 days, kept there for 16 days, and then quenched in cold water. Crystals of these ternary compounds are needle-shaped, and were found by semiquantitative energy-dispersive X-ray (EDX) analysis on a Hitachi S-2700 scanning electron microscope to contain all three elements in ratios consistent with the formulas obtained from the structure determinations (RE_3MnBi_5: observed 30−40% RE, 11−14% Mn, 45−55% Bi; expected 33% RE, 11% Mn, 56% Bi; $Sm_2Mn_3Bi_6$: observed 20−24% Sm, 23−28% Mn, 50−56% Bi; expected 18% Sm, 27% Mn, 56% Bi). Yields were typically greater than ∼95%, as ascertained by powder X-ray diffraction, with the most common byproduct being Bi.

Structure Determination. Single-crystal X-ray diffraction data were collected on a Bruker Platform/SMART 1000 CCD diffractometer using ω scans at −80 °C for RE_3MnBi_5 (RE = La−Nd) and at 22 °C for $Sm_2Mn_3Bi_6$. (Data were collected for RE_3MnBi_5 at low temperatures to investigate the possibility of phase transitions, which were not observed.) Structure solution and refinement were carried out with use of the SHELXTL (version 6.12) program package.[27] Face-indexed numerical absorption corrections were applied. Crystal data and further details of the data collections are given in Table 1.

For RE_3MnBi_5, the centrosymmetric space group *P*6$_3$/*mcm* was chosen and initial atomic positions were taken from related compounds adopting the inverse Hf_5Cu_3Sn-type structure.[20−26] For $Sm_2Mn_3Bi_6$, given that the Laue symmetry and systematic absences were consistent with the monoclinic space groups *P*2$_1$ and *P*2$_1$/*m*, the centrosymmetric space group *P*2$_1$/*m* was chosen and initial atomic positions were found by direct methods. Refinements proceeded in a straightforward manner, with all sites being fully occupied and having reasonable displacement parameters. Atomic positions were standardized with the program STRUCTURE TIDY.[28] Final values of the positional and displacement parameters are given in Tables 2 and 3. Selected interatomic distances are listed in Tables 4 and 5. Further data, in the form of a Crystallographic Information File (CIF), are available as Supporting Information or may be obtained from Fachinformationszentrum Karlsruhe, Abt. PROKA, 76344 Eggenstein-Leopoldshafen, Germany (Nos. CSD-418881 to 418884).

(15) Malik, S. K.; Chu, Z.; Joshi, A. G.; Yang, J. B.; Yelon, W. B.; Cai, Q.; James, W. J.; Kamaraju, K. *J. Appl. Phys.* **2002**, *91*, 7842−7844.
(16) Sologub, O.; Vybornov, M.; Rogl, P.; Hiebl, K.; Cordier, G.; Woll, P. *J. Solid State Chem.* **1996**, *122*, 266−272.
(17) Godart, C.; Rogl, P.; Alleno, E.; Gonçalves, A. P.; Rouleau, O. *Physica B* **2006**, *378*−*380*, 845−846.
(18) Bolotaev, A. G.; Koroliuk, A. L.; Morozkin, A. V.; Nikiforov, V. N. *J. Alloys Compd.* **2004**, *373*, L1−L2.
(19) Morozkin, A. V. *J. Alloys Compd.* **2005**, *395*, 7−16.
(20) Pecharsky, A. O.; Gschneidner, K. A., Jr. *J. Alloys Compd.* **1999**, *287*, 67−70.
(21) Brylak, M.; Jeitschko, W. *Z. Naturforsch. B: Chem. Sci.* **1994**, *49*, 747−752.
(22) Ferguson, M. J.; Hushagen, R. W.; Mar, A. *J. Alloys Compd.* **1997**, *249*, 191−198.
(23) Boulet, P.; Gross, G. M.; André, G.; Bourée, F.; Noël, H. *J. Solid State Chem.* **1999**, *144*, 311−317.
(24) Moore, S. H. D.; Deakin, L.; Ferguson, M. J.; Mar, A. *Chem. Mater.* **2002**, *14*, 4867−4873.
(25) Tkachuk, A. V.; Muirhead, C. P. T.; Mar, A. *J. Alloys Compd.* **2006**, *418*, 39−44.
(26) Mar, A.; Tougait, O.; Potel, M.; Noël, H.; Lopes, E. B. *Chem. Mater.* **2006**, *18*, 4533−4540.
(27) Sheldrick, G. M. *SHELXTL*, version 6.12; Bruker AXS Inc.: Madison, WI, 2001.
(28) Gelato, L. M.; Parthé, E. *J. Appl. Crystallogr.* **1987**, *20*, 139−143.

Table 2. Positional and Equivalent Isotropic Displacement Parameters ($Å^2$) for RE_3MnBi_5 (RE = La−Nd)[a]

	La_3MnBi_5	Ce_3MnBi_5	Pr_3MnBi_5	Nd_3MnBi_5
RE at 6*g* (*x*, 0, 1/4)				
x	0.61926(7)	0.61890(8)	0.61880(8)	0.61886(10)
U_{eq}	0.0101(2)	0.0101(2)	0.0095(2)	0.0074(2)
Mn at 2*b* (0, 0, 0)				
U_{eq}	0.0133(6)	0.0124(7)	0.0123(7)	0.0081(9)
Bi1 at 6*g* (*x*, 0, 1/4)				
x	0.25769(5)	0.25956(5)	0.26017(5)	0.26112(7)
U_{eq}	0.0103(1)	0.0099(2)	0.0094(2)	0.0068(2)
Bi2 at 4*d* (1/3, 2/3, 0)				
U_{eq}	0.0093(2)	0.0090(2)	0.0083(2)	0.0059(2)

[a] U_{eq} is defined as one-third of the trace of the orthogonalized U_{ij} tensor.

Table 3. Positional and Equivalent Isotropic Displacement Parameters for $Sm_2Mn_3Bi_6$[a]

atom	*x*	*z*	U_{eq}[b] ($Å^2$)
Sm1	0.06788(8)	0.32085(6)	0.0111(2)
Sm2	0.74760(8)	0.01308(6)	0.0105(2)
Mn1	0.4506(3)	0.3425(2)	0.0196(5)
Mn2	0.4645(3)	0.7624(2)	0.0187(5)
Mn3	0.7120(3)	0.2811(2)	0.0166(5)
Bi1	0.08119(6)	0.07811(5)	0.0113(1)
Bi2	0.16569(6)	0.79441(5)	0.0127(1)
Bi3	0.37025(7)	0.53820(5)	0.0193(2)
Bi4	0.47860(6)	0.10213(5)	0.0124(1)
Bi5	0.73670(6)	0.74283(5)	0.0136(1)
Bi6	0.88642(6)	0.48995(5)	0.0140(1)

[a] All atoms are in Wyckoff position 2*e* (*x*, 1/4, *z*). [b] U_{eq} is defined as one-third of the trace of the orthogonalized U_{ij} tensor.

Table 4. Selected Interatomic Distances (Å) in RE_3MnBi_5 (RE = La, Ce, Pr, Nd)

	La_3MnBi_5	Ce_3MnBi_5	Pr_3MnBi_5	Nd_3MnBi_5
RE−Bi1 (×2)	3.2690(7)	3.2446(6)	3.2338(7)	3.2213(9)
RE−Bi2 (×4)	3.4404(4)	3.4087(3)	3.3967(4)	3.3830(6)
RE−Bi1 (×2)	3.4573(4)	3.4268(4)	3.4184(5)	3.4030(6)
RE−Bi1	3.5123(9)	3.4579(9)	3.4374(10)	3.4142(13)
RE−RE (×2)	3.9866(9)	3.9511(9)	3.9403(9)	3.9263(12)
Mn−Bi1 (×6)	2.9828(5)	2.9719(5)	2.9671(5)	2.9627(6)
Mn−Mn (×2)	3.2441(4)	3.2210(3)	3.2156(4)	3.2044(5)
Bi2−Bi2 (×2)	3.2441(4)	3.2210(3)	3.2156(4)	3.2044(5)

Table 5. Selected Interatomic Distances (Å) in $Sm_2Mn_3Bi_6$

Sm1−Bi1	3.2687(10)	Mn2−Bi4 (×2)	2.810(2)
Sm1−Bi6 (×2)	3.2808(7)	Mn2−Bi3	2.831(3)
Sm1−Bi5 (×2)	3.2960(7)	Mn2−Bi5	2.919(3)
Sm1−Bi2 (×2)	3.3015(8)	Mn2−Bi2	3.262(3)
Sm1−Bi6	3.3492(10)	Mn3−Bi6	2.805(3)
Sm1−Bi3	3.5490(11)	Mn3−Bi4	2.823(3)
Sm2−Bi4 (×2)	3.2566(7)	Mn3−Bi2 (×2)	2.893(2)
Sm2−Bi2 (×2)	3.2994(7)	Mn1−Mn2 (×2)	2.905(3)
Sm2−Bi1	3.3032(10)	Mn1−Mn3	3.069(4)
Sm2−Bi1 (×2)	3.3056(7)	Mn2−Mn3 (×2)	2.830(2)
Sm2−Bi4	3.3551(10)	Bi1−Bi1 (×2)	3.1544(8)
Sm2−Bi5	3.5553(10)	Bi1−Bi5 (×2)	3.3787(7)
Mn1−Bi5 (×2)	2.945(2)	Bi3−Bi6 (×2)	3.4060(7)
Mn1−Bi3	2.965(3)	Bi4−Bi4 (×2)	3.6421(10)
Mn1−Bi3 (×2)	3.019(2)	Bi6−Bi6 (×2)	3.1964(9)
Mn1−Bi4	3.294(3)		

Band Structure. For La_3MnBi_5, tight-binding linear muffin tin orbital (TB-LMTO) band structure calculations were performed within the local density and atomic spheres approximations using the Stuttgart TB-LMTO program.[29] The basis sets consisted of La 6s/6p/5d/4f, Mn 4s/4p/3d, and Bi 6s/6p/6d/5f orbitals, with the La 6p and Bi 6d/5f orbitals being downfolded. Integrations in reciprocal space were carried out with an improved tetrahedron method over 95 irreducible *k* points.

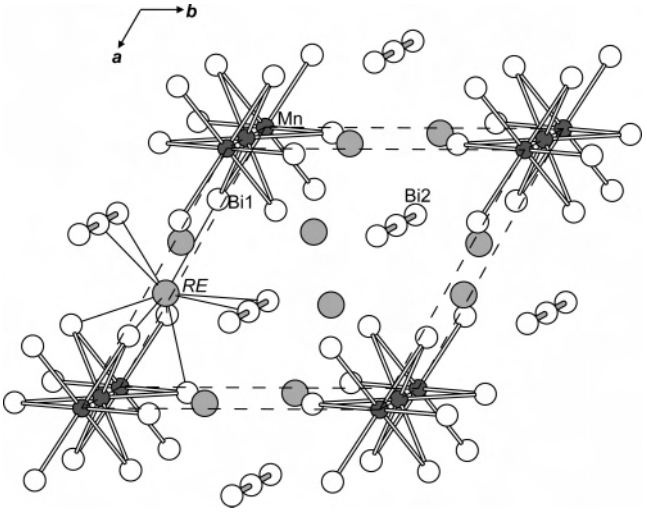

Figure 1. Structure of RE_3MnBi_5 (RE = La−Nd) viewed down the *c* direction. The large lightly shaded circles are RE atoms, the small solid circles are Mn atoms, and the medium open circles are Bi atoms.

For $Sm_2Mn_3Bi_6$, difficulties were encountered in reaching convergence when LMTO methods were applied. Instead, tight-binding extended Hückel band structure calculations were performed with the EHMACC suite of programs,[30,31] on the $[Mn_3Bi_6]^{6-}$ part of $Sm_2Mn_3Bi_6$, with Hückel parameters taken from previous calculations on La_6MnSb_{15} and Ti_4MnBi_2.[32,33] Qualitative results of this calculation are presented in the Supporting Information (Figure S1).

Electrical and Magnetic Properties. Needle-shaped single crystals of RE_3MnBi_5 (RE = La−Nd) and $Sm_2Mn_3Bi_6$, whose identities were confirmed by EDX analyses, were mounted for electrical resistivity measurements, made between 2 and 300 K by standard four-probe techniques on a Quantum Design PPMS system equipped with an ac transport controller (Model 7100). The current was 100 μA and the frequency was 16 Hz. The resistivity was measured along the needle axis of the crystals, which corresponds to the crystallographic *c*-axis for RE_3MnBi_5 or the *b*-axis for $Sm_2Mn_3Bi_6$. All measurements were repeated at least twice.

Measurements of dc magnetic susceptibilities were made on ground samples (~60−120 mg) between 2 and 300 K on a Quantum Design 9T-PPMS dc magnetometer/ac susceptometer. Susceptibility values were corrected for contributions from the holder and sample diamagnetism. Measurements of ac magnetic susceptibility were made with a driving amplitude of 1 Oe and a frequency of 1000 Hz. Magnetic properties of Ce_3MnBi_5 have been reported previously[20] and were not examined further here.

Results and Discussion

Structure. Although there are now many examples of ternary f-element antimonides such as RE_3MSb_5 (RE = rare earth; M = Ti, Zr, Hf, Nb)[22,24] and U_3MSb_5 (M = Sc, Ti, Zr, Hf, V, Nb, Ta, Cr, Mn)[21,25,26] that adopt the inverse

(29) Tank, R.; Jepsen, O.; Burkhardt, A.; Andersen, O. K. *TB-LMTO-ASA program*, version 4.7; Max Planck Institut für Festkörperforschung: Stuttgart, 1998.

(30) Whangbo, M.-H.; Hoffmann, R. *J. Am. Chem. Soc.* **1978**, *100*, 6093−6098.

(31) Hoffmann, R. *Solids and Surfaces: A Chemist's View of Bonding in Extended Structures*; VCH Publishers: New York, 1988.

(32) Papoian, G.; Hoffmann, R. *J. Solid State Chem.* **1998**, *139*, 8−21.

(33) Rytz, R.; Hoffmann, R. *Inorg. Chem.* **1999**, *38*, 1609−1617.

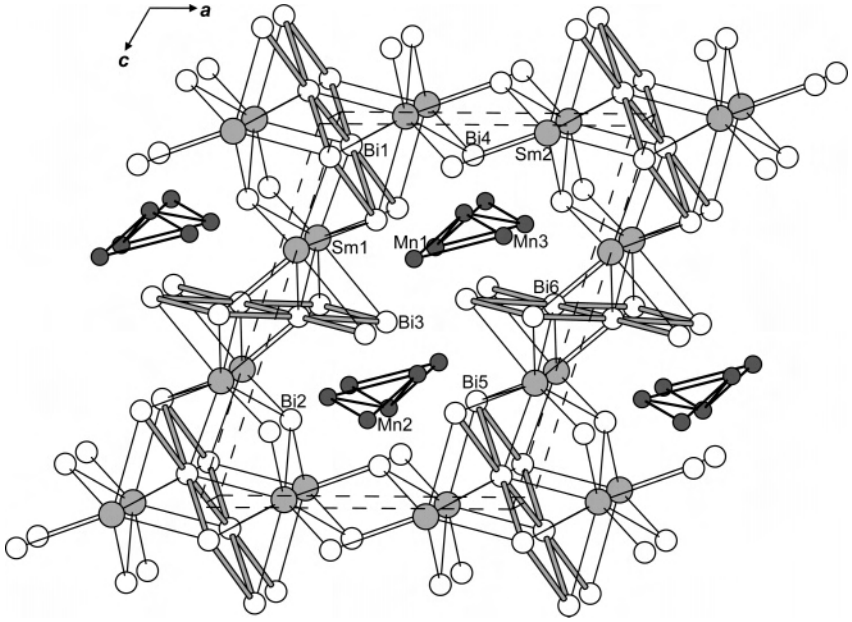

Figure 2. Structure of $Sm_2Mn_3Bi_6$ viewed down the *b* direction. The large lightly shaded circles are Sm atoms, the small solid circles are Mn atoms, and the medium open circles are Bi atoms.

Hf_5Cu_3Sn-type structure, the only bismuth representatives known so far are La_3MBi_5 (M = Mg, Sc)[34,35] and Ce_3MnBi_5.[20] Here, we have shown that the degree of rare-earth substitution in the RE_3MnBi_5 series extends to RE = La, Ce, Pr, and Nd. Proceeding further along the rare earths, we were unable to prepare "Sm_3MnBi_5" but have discovered instead the new compound $Sm_2Mn_3Bi_6$.

In the structure of RE_3MnBi_5, chains of face-sharing Mn-centered octahedra and skewers of Bi2 atoms are aligned along the *c* direction, separated by RE atoms in roughly tricapped trigonal prismatic coordination (Figure 1). The cell parameters, as well as the RE−Bi and RE−RE distances, decrease monotonically in accordance with the lanthanide contraction on going from RE = La to Nd. The Mn-centered octahedra become slightly more squashed along the *c* direction on going from La_3MnBi_5 (Bi1−Mn−Bi1 angles of 86.77(1)° and 93.23(1)°) to Nd_3MnBi_5 (Bi1−Mn−Bi1 angles of 86.49(1)° and 93.51(1)°). Consistent with the greater coordination number, the Mn−Bi1 distances within these octahedra (CN6) (2.9828(5)−2.9627(6) Å) are longer than those within the Mn-centered tetrahedra (CN4) in $Eu_{14}MnBi_{11}$ (2.862(1) Å)[7] or $Yb_{14}MnBi_{11}$ (2.803(1) Å).[8] Although the Bi2−Bi2 distances within the linear skewers (3.2441(4)−3.2044(5) Å) are longer than the sum of the metallic radii (3.020 Å)[36] or the intralayer distance in elemental Bi (3.072 Å),[37] they are shorter than the interlayer distance in Bi (3.529 Å),[37] where weak bonding interactions are still implicated. On the other hand, the Mn−Mn distances within face-sharing octahedra are quite long (3.2441(4)−3.2044(5) Å) and it is not obvious if metal−metal bonding is operative. Normally, the presence of face-sharing octahedra is disfavored by cation−cation repulsions, unless an overriding factor like metal−metal bonding stabilizes this arrangement. Because the Bi−Bi and Mn−Mn distances are necessarily identical (equal to half the *c* parameter), an interesting question is whether one set of distances is defined merely because of matrix effects imposed by the other set. In this regard, overlap populations obtained from band structure calculations (vide infra) will prove helpful in revealing if these distances correspond to real bonding interactions.

$Sm_2Mn_3Bi_6$ adopts a new monoclinic structure type. A convenient way to build up this structure is through the linking of Sm-centered polyhedra, creating channels along the *b* direction that are occupied by chains of Mn atom clusters (Figure 2). Each of the two types of Sm atoms is ninefold coordinated by Bi atoms in monocapped square antiprismatic geometry, with the capping atom tilted slightly to one side (Figure 3). The lower limit of the Sm−Bi distances (3.2566(7)−3.5553(10) Å) in $Sm_2Mn_3Bi_6$ already exceeds the shortest RE−Bi distance found in Nd_3MnBi_5 (3.2213(9) Å), suggesting that the RE_3MnBi_5 series ceases beyond RE = Nd because of increasingly severe size mismatch of the RE atoms within the structure. A remarkable feature of $Sm_2Mn_3Bi_6$ is the presence of three types of Mn-centered polyhedra, in diverse coordination geometries: distorted octahedral (CN6), trigonal bipyramidal (CN5), and distorted tetrahedral (or seesaw) (CN4) (Figure 4). The Mn atoms are also separated by Mn−Mn distances (2.830(2)−3.069(4) Å), shorter than in RE_3MnBi_5, which may be suggestive of weak bonding interactions. Finally, the Bi atoms are arranged in two types of four-atom-wide ribbons extending along the *b* direction with alternately short and long Bi−Bi distances across the width: Bi3−Bi6−Bi6−Bi3

(34) Pan, D.-C.; Sun, Z.-M.; Mao, J.-G. *J. Solid State Chem.* **2006**, *179*, 1016−1021.
(35) Pan, D.-C.; Sun, Z.-M.; Lei, X.-W.; Mao, J.-G. *Chin. J. Inorg. Chem.* **2006**, *22*, 1449−1452.
(36) Pauling, L. *The Nature of the Chemical Bond*, 3rd ed.; Cornell University Press: Ithaca, NY, 1960.
(37) Donohue, J. *The Structures of the Elements*; Wiley: New York, 1974.

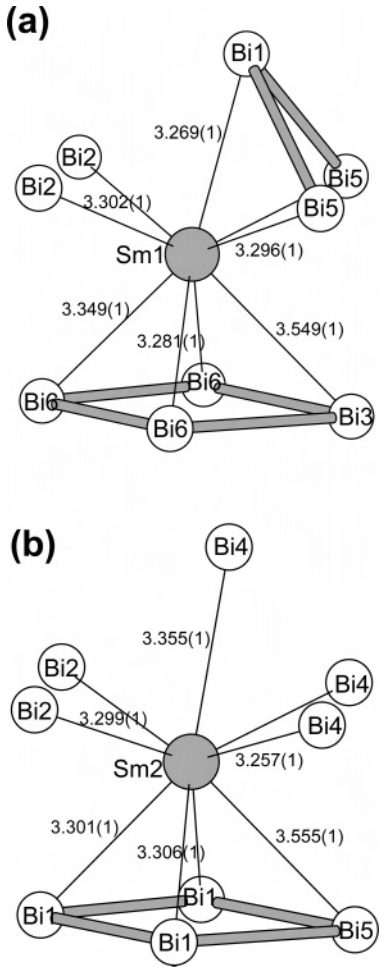

Figure 3. Coordination around (a) Sm1 and (b) Sm2 atoms in $Sm_2Mn_3Bi_6$.

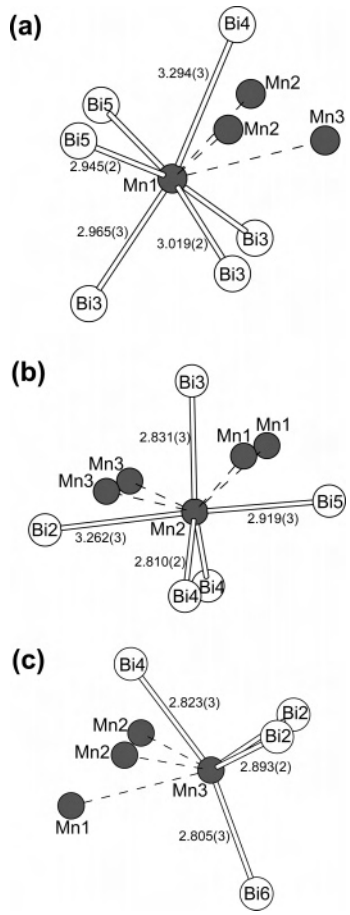

Figure 4. Coordination around (a) Mn1, (b) Mn2, and (c) Mn3 atoms in $Sm_2Mn_3Bi_6$.

(lying parallel to the (001) plane) and Bi5−Bi1−Bi1−Bi5 (lying parallel to the (10$\bar{1}$) plane) (Figure 5). These polyanionic substructures can be imagined to be excised from infinite square nets of pnicogen atoms,[1] a recurring motif in the structures of polyantimonides and, now, polybismuthides.

Despite its complexity, the structure of the ternary bismuthide $Sm_2Mn_3Bi_6$ can be related in an interesting way to the simpler structure of the binary antimonide $SmSb_2$,[38] both being built up from monocapped square antiprismatic polyhedra centered by the Sm atoms. In the orthorhombic structure of $SmSb_2$, the monocapped square antiprisms are connected to form stacked slabs demarcated by square Sb sheets (Figure 6a). Removing every third Sm atom from $SmSb_2$ in an ordered manner results in a hypothetical vacancy-ordered "$Sm_2\square Sb_6$" structure (Figure 6b). Displacing some of the Sb atoms in the square sheets in "$Sm_2\square Sb_6$" toward the vacancies as well as shifting the capping Sb atoms slightly then reproduces the "Sm_2Bi_6" framework in $Sm_2Mn_3Bi_6$ (Figure 6c). Finally, the vacancies are filled by Mn_3 clusters, which are arranged in chains within channels along the *b* direction in $Sm_2Mn_3Bi_6$ (Figure 6d).

Bonding. The occurrence of polyanionic Bi substructures, in the form of linear chains in RE_3MnBi_5 and four-atom-wide ribbons in $Sm_2Mn_3Bi_6$, is reminiscent of similar features in antimonides.[1] Linear chains of pnicogen atoms are also found in polyantimonides, where hypervalent Sb−Sb bond-

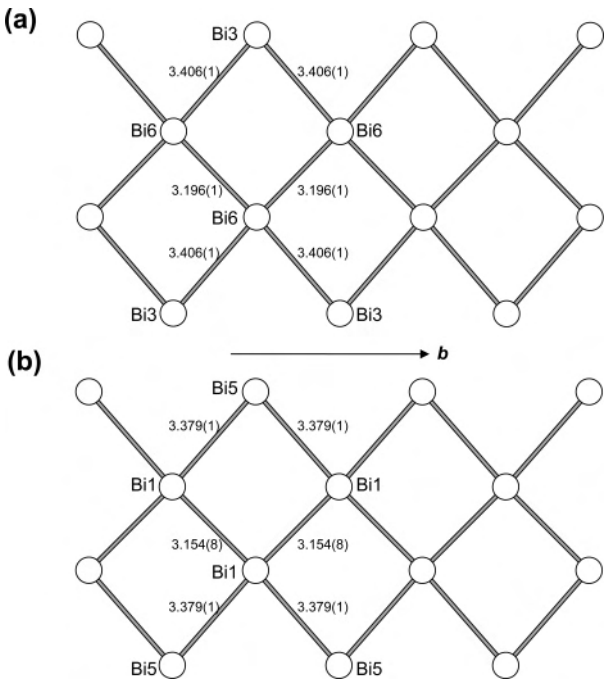

Figure 5. Four-atom-wide Bi ribbons extended along the *b* direction, lying nearly parallel to the (a) (001) plane or (b) (10$\bar{1}$) plane in $Sm_2Mn_3Bi_6$.

(38) Wang, R.; Steinfink, H. *Inorg. Chem.* **1967**, *6*, 1685−1692.

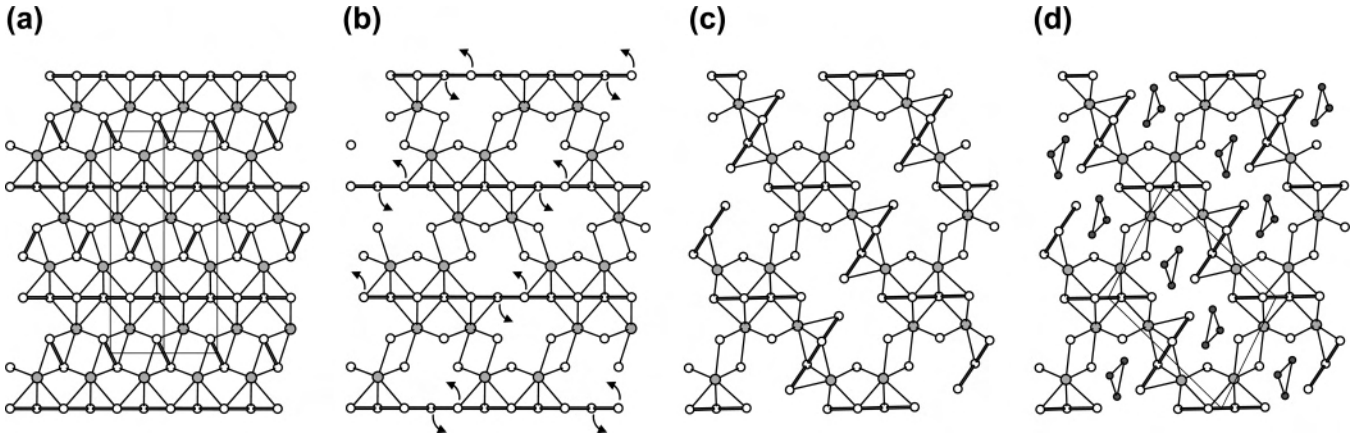

Figure 6. Structural evolution from $SmSb_2$ to $Sm_2Mn_3Bi_6$. Every third Sm atom is removed from $SmSb_2$ in (a), yielding a vacancy-ordered "$Sm_2\square Sb_6$" structure in (b), where some of the pnicogen atoms in square sheets are then displaced to give (c). Then, chains of Mn_3 clusters are inserted within the empty channels to give the structure of $Sm_2Mn_3Bi_6$ in (d).

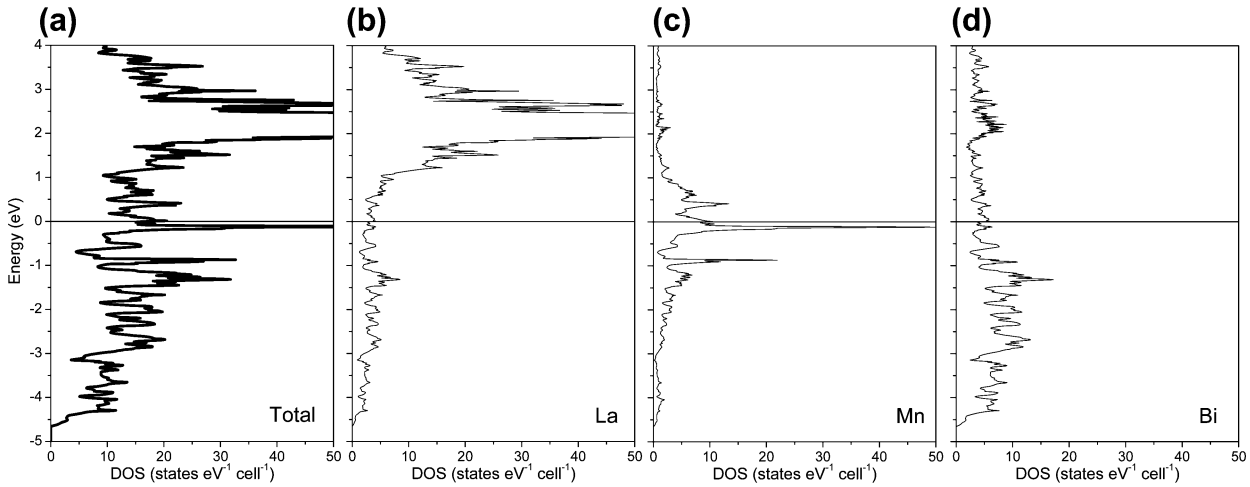

Figure 7. (a) Total density of states (DOS) for La_3MnBi_5 and its (b) La, (c) Mn, and (d) Bi contributions. The Fermi level is marked by a horizontal line at 0 eV.

ing is invoked.[39] A two-bonded Pn atom within such a chain is assigned a formal charge of Pn^{2-}, with three lone pairs counted on each atom and each Pn−Pn interaction approximated as a one-electron bond. Although trivalent RE is essentially certain in these compounds, the valence state of Mn is not necessarily obvious. For RE_3MnBi_5, a Zintl-type formulation $(RE^{3+})_3(Mn^{4+})(Bi1^{3-})_3(Bi2^{2-})_2$ accounts handily for the bonding and is consistent with previous magnetic measurements on Ce_3MnBi_5.[20] Of course, charge transfer as extreme as this does not occur in reality and instead will be even less pronounced in these bismuthides than in the antimonides. Although the density of states calculated for La_3MnBi_5 does show mostly unoccupied La states, there is significant mixing of Mn and Bi states implying considerable covalent character to the bonding (Figure 7). As seen in the crystal orbital Hamiltonian population (COHP) curves (Figure 8), these Mn−Bi interactions are strongly bonding (with an integrated −COHP of 1.19 eV/bond). Interestingly, even the long (∼3.2 Å) Mn−Mn interactions within the face-sharing octahedral chains are found to be non-innocent (−ICOHP of 0.38 eV/bond). The equally long Bi−Bi interactions within the linear chains also correspond to net bonding (−ICOHP of 0.53 eV/bond). For all three types of interactions, some antibonding levels are occupied at the Fermi level. If a rigid band structure is assumed, depopulation of these levels to strengthen the bonding could be achieved through substitution of Mn by a metal with fewer electrons such as Cr. To date, no ternary RE−Cr−Bi phases have been reported.

For $Sm_2Mn_3Bi_6$, the wide variety of intermediate homoatomic interactions makes it more difficult to formulate charge assignments. As first applied by Jeitschko et al. to binary rare-earth polyantimonides,[40] bond valence calculations can provide approximate nonintegral formal charges on pnicogen atoms involved in such interactions. The bond order is given by the equation $\nu_{ij} = \exp[(R_{ij} - d_{ij})/0.37]$, where R_{ij} is the bond valence parameter and d_{ij} is the distance in Å.[41] Examining all d_{ij} values shorter than 4.0 Å and

(39) Papoian, G. A.; Hoffmann, R. *Angew. Chem., Int. Ed.* **2000**, *39*, 2409−2448.

(40) Jeitschko, W.; Altmeyer, R. O.; Schelk, M.; Rodewald, U. Ch. *Z. Anorg. Allg. Chem.* **2001**, *627*, 1932−1940.

(41) Brown, I. D. In *Structure and Bonding in Crystals*; O'Keeffe, M., Navrotsky, A., Eds.; Academic Press: New York, 1981; Vol. 2, pp 1−30.

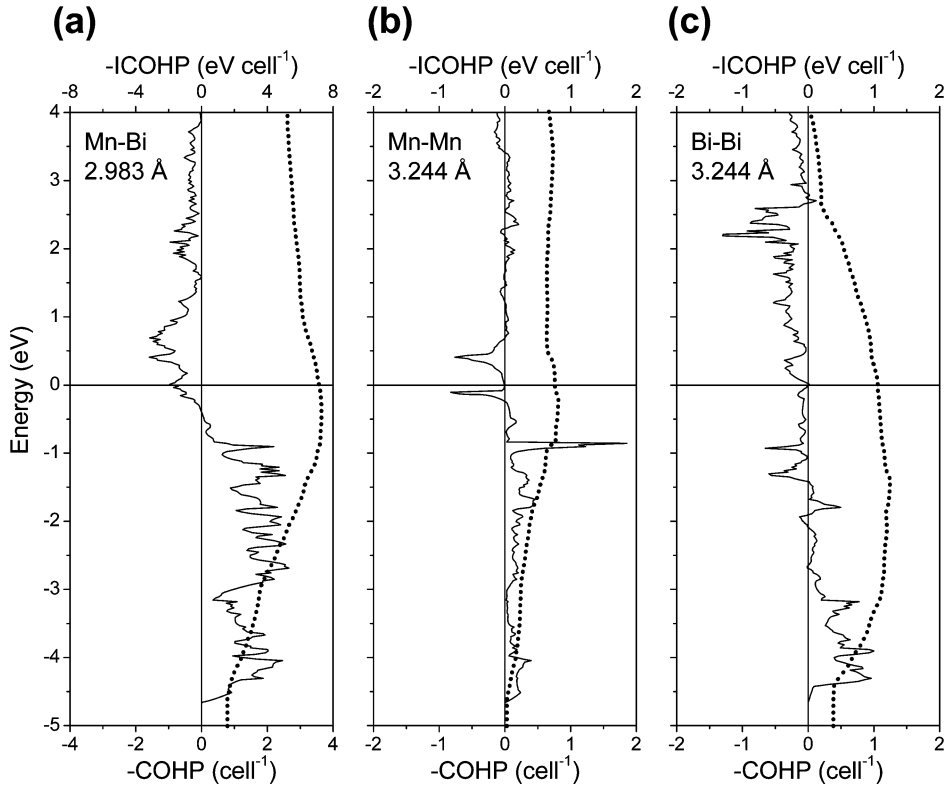

Figure 8. Crystal orbital Hamilton population (COHP) curves (solid line) and integrated COHP curves (dotted line) for (a) Mn−Bi, (b) Mn−Mn, and (c) Bi−Bi contacts in La_3MnBi_5. The Fermi level is marked by a horizontal line at 0 eV.

choosing an R_{ij} value of 3.06 Å, with the assumption that the R_{ij} value listed by O'Keeffe and Brese[42] for Bi−Bi interactions (3.08 Å) is overestimated by the same amount (0.02 Å) as for Sb−Sb interactions, we obtain formal charges of −0.6 for Bi1, −3.0 for Bi2, −1.8 for Bi3, −2.6 for Bi4, −2.1 for Bi5, and −0.8 for Bi6. The total formal charge for all the Bi atoms is then −11 per formula unit of $Sm_2Mn_3Bi_6$, which is close to a compensating positive charge of +12 assuming two Sm^{3+} and three Mn^{2+} atoms. A simpler method is to assign "interior" Bi atoms to be −1 and "border" Bi atoms to be −2 within the four-atom-wide Bi ribbons, similar to what we have proposed elsewhere for Sb ribbons,[1] and regard all remaining isolated Bi atoms as monoanions with a charge of −3. The formal charges obtained in this manner (−1 for Bi1, −3 for Bi2, −2 for Bi3, −3 for Bi4, −2 for Bi5, and −1 for Bi6) then sum up to exactly −12. An extended Hückel band structure calculation (on the $[Mn_3Bi_6]^{6-}$ part of $Sm_2Mn_3Bi_6$) lends qualitative support for the presence of these weak Bi−Bi interactions (Figure S1 in Supporting Information), which correspond to a nonnegligible Mulliken overlap population of 0.31. Moreover, the different types of Bi atoms can be weakly discriminated by their atomic orbital populations, with the isolated Bi2 atoms being most reduced and the Bi1 and Bi6 atoms within the interior of the four-atom-wide ribbons being least reduced. Last, the Mn−Mn interactions within the Mn_3 clusters are confirmed to be weakly bonding, with an overlap population of 0.09.

(42) O'Keeffe, M.; Brese, N. E. *J. Am. Chem. Soc.* **1991**, *113*, 3226−3229.

Properties. Figure 9 shows plots of the electrical resistivity of RE_3MnBi_5 and $Sm_2Mn_3Bi_6$, which generally decrease as the temperature is lowered, indicating metallic behavior. The resistivity profiles for RE_3MnBi_5 (RE = La, Nd, Pr) are similar, showing only a weak, nearly linear temperature dependence at high temperatures but then decreasing dramatically below ∼40 K (Figure 9a). This behavior is similar to that seen in U_3MSb_5 (M = Zr, Hf, Nb), where the transitions occur at higher temperatures (115−145 K) and coincide with the onset of ferromagnetic ordering.[25] The resistivity for Ce_3MnBi_5 has been measured for the first time here, and its profile is distinctly different, exhibiting a maximum near ∼50 K before the resistivity falls rapidly again. (The high-temperature feature above ∼250 K is probably a spurious artifact of this measurement, but the 50 K maximum has been observed in multiple measurements on several crystals of Ce_3MnBi_5. In general, there is a shallow minimum centered near 225 K.) This behavior is reminiscent of Ce-containing intermetallics that are Kondo-lattice materials. Interestingly, previous measurements on Ce_3MnBi_5 also indicated a deviation in the magnetic susceptibility from the Curie−Weiss law below ∼50 K and a maximum in the C_p/T vs T plot at ∼40 K.[20] Unlike the RE_3MnBi_5 compounds, the resistivity of $Sm_2Mn_3Bi_6$ shows a pronounced downward curvature but a much less dramatic drop at lower temperature (Figure 9b).

Figure 10 shows plots of magnetic data for phase-pure samples of Pr_3MnBi_5 and Nd_3MnBi_5. (Data for La_3MnBi_5 and $Sm_2Mn_3Bi_6$ samples, whose purities are less certain, have been relegated to Supporting Information. Fitting of the high-

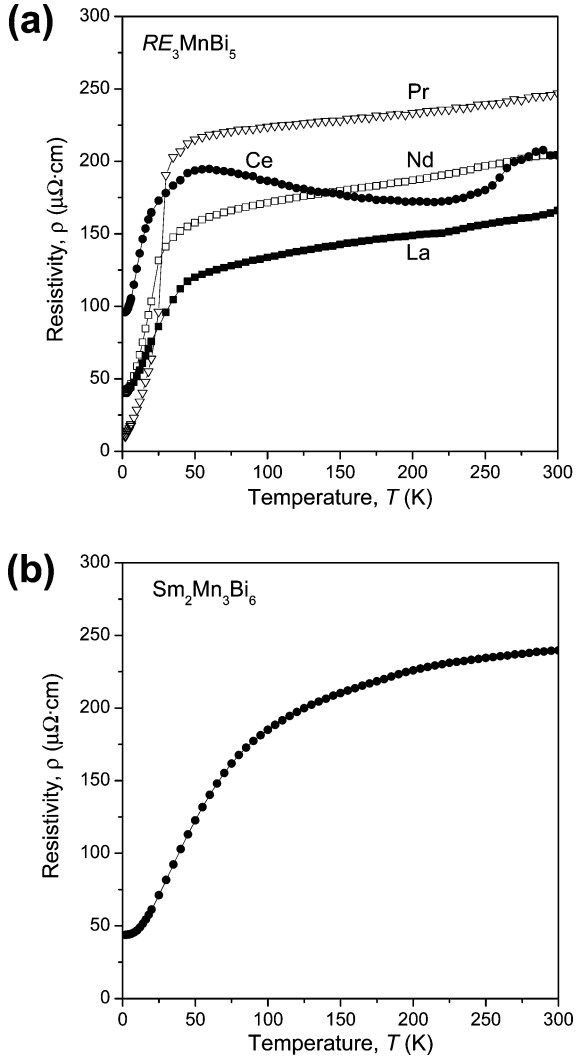

Figure 9. Electrical resistivity of single crystals of (a) RE_3MnBi_5 (RE = La−Nd) and (b) $Sm_2Mn_3Bi_6$.

temperature magnetic susceptibility data for La_3MnBi_5 to the modified Curie−Weiss law gave $\mu_{eff} = 3.87(5)\ \mu_B$/formula unit (f.u.), apparently in excellent agreement with the free-ion value for Mn^{4+} ($3d^3$) and the Zintl formulation $(La^{3+})_3(Mn^{4+})(Bi1^{3-})_3(Bi2^{2-})_2$ discussed earlier. $Sm_2Mn_3Bi_6$ shows non-Curie−Weiss behavior typical of Sm-containing compounds in which low-lying excited states are available.) The magnetic susceptibility of Pr_3MnBi_5 increases rapidly below ~25 K (Figure 10a), indicative of magnetic ordering. A fit of the high-temperature data to the modified Curie−Weiss law, $\chi = C/(T - \theta_p) + \chi_o$ (inset of Figure 10a), gave parameters of $\mu_{eff} = 5.9(1)\ \mu_B$/f.u., $\theta_p = -72(4)$ K, and $\chi_o = 0.0068(3)$ emu/mol. The large negative value of θ_p indicates antiferromagnetic coupling which, in conjunction with the rapid upturn in the magnetic susceptibility, suggests a ferrimagnetic spin arrangement of the Pr and Mn moments. The large temperature-independent term in the Curie−Weiss fit also suggests important contributions from conduction electrons to the magnetic susceptibility. The isothermal magnetization at 2 K (Figure 10b) reveals an approach to saturation behavior below the ordering temperature, which was confirmed from ac susceptibility measurements to be at

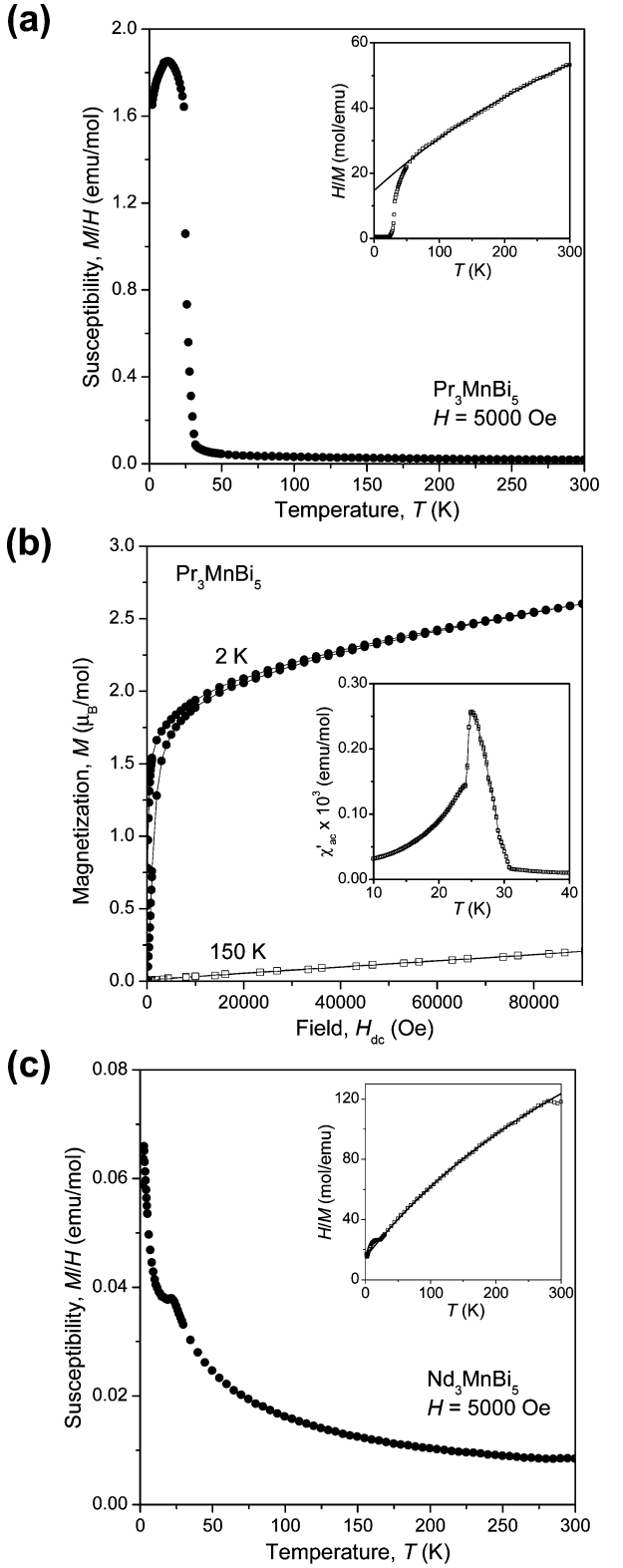

Figure 10. Magnetic data for (a)−(b) Pr_3MnBi_5 and (c) Nd_3MnBi_5. In (a) and (c), the inverse susceptibility and fits to the modified Curie−Weiss law are shown in the insets. In (b), isothermal magnetization curves and the real component of the ac magnetic susceptibility (inset) for Pr_3MnBi_5 are shown.

25 K (inset of Figure 10b). In contrast, Nd_3MnBi_5 shows paramagnetic behavior ($\mu_{eff} = 3.64(2)\ \mu_B$/f.u., $\theta_p = -25(1)$ K, $\chi_o = 0.0030(1)$ emu/mol), with an anomaly at 20 K that, at first glance, could be dismissed as a contribution from an

unidentified impurity phase (Figure 10c). However, it is interesting to note that in Pr_3MnBi_5 and Nd_3MnBi_5, the transitions in the magnetic susceptibility (measured on powder samples) (Figure 10) coincide (within ~10 K) with those in the electrical resistivity (measured on single crystals) (Figure 9), suggesting that they are intrinsic to the compounds themselves and not to an impurity phase. The rapid decrease in resistivity is often associated with the loss of spin-disorder scattering as some type of magnetic ordering sets in.

Conclusions

Although Bi is considered to be a metal and normally adopts positive oxidation states (e.g., in oxides and halides), it may undergo very little electron transfer (in intermetallic compounds) or indeed, under favorable circumstances, be prone to accept electron density from more electropositive elements to form polyanionic networks. Such bismuthides can been found in combination with alkali metals (e.g., A_3Bi_2),[43] but representatives involving the less electropositive rare-earth metals are less likely (e.g., $LaGaBi_2$).[2] The compounds presented here, RE_3MnBi_5 (RE = La−Nd) and $Sm_2Mn_3Bi_6$, represent genuine examples of polybismuthides. The one-dimensional chains of Bi atoms in RE_3MnBi_5 and the four-atom-wide Bi ribbons in $Sm_2Mn_3Bi_6$ appear to follow similar electron-counting rules as found in hypervalent polyantimonide networks. Preliminary analysis with X-ray photoelectron spectroscopy on La_3MnBi_5 and Pr_3MnBi_5, made on a Kratos AXIS 165 spectrometer, indicate that the Bi $4f_{7/2}$ and $4f_{5/2}$ peaks shift to lower binding energies relative to those in elemental bismuth by 0.2−0.3 eV, consistent with the presence of anionic Bi and with analogous shifts observed in polyantimonides.[44] Property measurements indicate that these are metallic compounds that undergo magnetic ordering at modest temperatures. Neutron diffraction studies are in progress to determine the magnetic structures of some of these compounds in detail.

Acknowledgment. The Natural Sciences and Engineering Research Council of Canada and the University of Alberta supported this work. We thank Dr. Robert McDonald and Dr. Michael J. Ferguson (X-ray Crystallography Laboratory) for the X-ray data collection, Ms. Christina Barker (Department of Chemical and Materials Engineering) for assistance with the SEM−EDX analysis, and Mr. Andrew P. Grosvenor for the XPS analysis.

Supporting Information Available: X-ray crystallographic files in CIF format, one figure showing band structure calculations on the $[Mn_3Bi_6]^{6-}$ part of $Sm_2Mn_3Bi_6$, and one figure showing additional magnetic data for La_3MnBi_5 and $Sm_2Mn_3Bi_6$. This material is available free of charge via the Internet at http://pubs.acs.org.

IC701428P

(43) Gascoin, F.; Sevov, S. C. *J. Am. Chem. Soc.* **2000**, *122*, 10251−10252.

(44) Grosvenor, A. P.; Cavell, R. G.; Mar, A. *Phys. Rev. B* **2006**, *74*, 125102-1−125102-10.